6 Dynamics of water molecules in an alkaline environment

We report on two-color mid-infrared pump–probe spectroscopy experiments on the OH stretch vibration of HDO molecules in a concentrated (10 M) solution of NaOD in D_2O. The results indicate that the broad absorption band consists of two separate classes of OH groups: (I) OH groups with $DO-H\cdots OD_2$-like hydrogen bonds, surprisingly similar to those in HDO:D_2O. (II) OH groups with $DO-H\cdots OD^-$-like hydrogen bonds, which show a very rapid vibrational relaxation, possibly due to deuteron transfers. For component I, the lifetime of the OH stretch vibration is observed to increase with frequency, which can be explained from the accompanying decrease in the strength of the hydrogen-bond interaction. Spectral holes can be created that change neither position nor width on a picosecond timescale. This behavior differs strongly from that of pure HDO:D_2O where rapid spectral diffusion ($\tau \approx 600$ fs) occurs. The spectral inhomogeneity indicates that, in this solution, the hydrogen bond network is very static.

6.1 Introduction

It is well-known that in solutions of salts in water, the ions are embedded in a shell that consists of a small number of water molecules. The presence of these solvation shells has a strong effect on the structure of the hydrogen-bond network that links the water molecules. For this reason, ions have been categorized as either structure-breaking or structure-making.[30,125,126] More recently, experiments showed that water molecules in the solvation shells of negative ions (e.g. Cl^-) behave very differently from those in bulk water.[62] For example, the hydrogen bond length $DO-H\cdots Cl^-$ varies on a much slower time scale (∼12 ps) than the otherwise comparable hydrogen bond $DO-H\cdots OD_2$ between two water molecules (∼600 fs).[33,129]

An interesting question is what happens if the negative ion is a base B^- that can accept protons or deuterons from neighboring water molecules according to

$$HO-H\cdots B^- \rightarrow HO^-\cdots H-B. \tag{6.1}$$

Even for a weak base, the hydrogen bond between water and the base ion is much stronger than that among water molecules or between water molecules and halide ions. As a result, the difference between the hydrogen bond and the covalent O–H bond gets blurred. A special example of this blurring is when the left and right side of the reaction [Eq. (6.1)] are identical, which happens if the base is a hydroxyl (OH^-) ion.

Figure 6.1 shows the infrared absorption spectrum of OH groups in a 10 mol/l NaOD in D_2O solution in which a small fraction of D atoms is substituted by H atoms. Here, we obtain a mixture (further denoted as 'NaOX solution') containing OH groups both in OH^- ions and in HDO molecules. The high concentration of OD^- ions has a remarkable

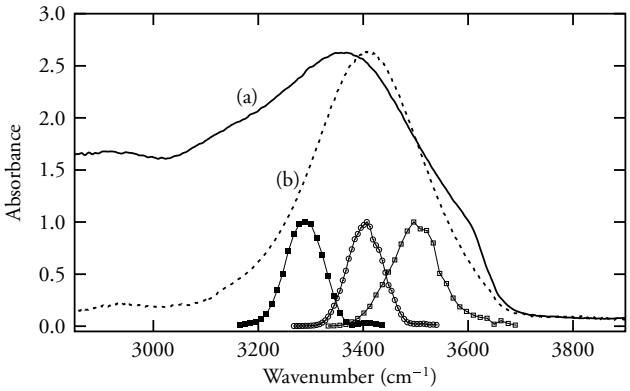

FIGURE 6.1. Absorbance ($= -\ln(T_o)$) spectra of O–H groups in (a) 10 M NaOD in D_2O in which a small fraction of D atoms is substituted by H atoms (referred to as NaOX solution). A background of a pure (unsubstituted) sample was substracted. For comparison, (b) shows the spectrum of OH groups in HDO:D_2O. The small curves on the bottom indicate the excitation spectra used in the experiments.

effect on the OH stretch absorption band, compared to the case of HDO in D_2O (§1.1 and other chapters), with an OH stretch absorption spectrum that has a width of 270 cm^{-1} and a central frequency of 3405 cm^{-1}. Compared to water, the spectrum of the NaOX solution is strongly broadened towards lower frequencies, and shows a shoulder around 3600 cm^{-1}.

The very broad absorption spectrum of the NaOX solution is not understood in detail, but has been interpreted as follows.[38,108] The Na^+ ions have no direct effect on the OH stretch spectrum, because water molecules do not form hydrogen bonds with these positive ions. In contrast, the OX^- ions are embedded in the hydrogen-bond network, and the OH groups can have many possible configurations with respect to their direct environment. Roughly, we can distinguish three categories for these OH groups. In the range 3200–3500 cm^{-1}, we see the majority of HDO molecules, which donate hydrogen bonds to other HDO or D_2O molecules (as in Fig. 6.2a). This is comparable to the situation of HDO dissolved in D_2O (compare the spectra in Fig. 6.1a), except that the central frequency is shifted to a somewhat lower value. This means that hydrogen bonds are, on the average, shorter (and stronger) in the NaOX solution than in HDO:D_2O. This is not surprising, given the overall higher density of oxygen atoms at this NaOD concentration (62 mol/l, compared to 56 mol/l in plain water).

At lower frequencies, the absorption results from HDO molecules that form strong hydrogen bonds with OD^- ions (Fig. 6.2b). Depending on the exact geometry and the relevant interactions, the complex may also be described as an $HD_4O_3^-$, $HD_6O_4^-$, or $HD_8O_5^-$ complex.[108,118,119,123,127] The OD^- ion can easily accept protons or deuterons from neighboring HDO or D_2O molecules.

Finally, the shoulder at 3600 cm^{-1} is attributed to the OH^- ions (Fig. 6.2c). OH^- ions are only weak donors of hydrogen bonds because of their negative charge.[118] The resulting length and weakness of the $OH^- \cdots OD_2$ hydrogen bonds[118,127] cause their frequency to be rather high.[38]

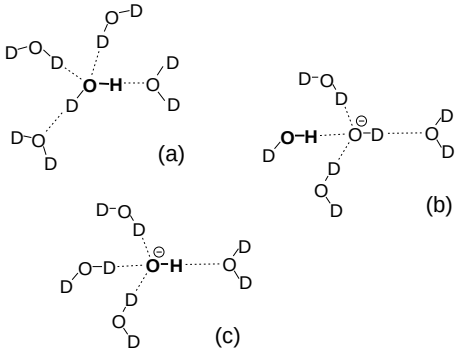

FIGURE 6.2. Different classes of OH groups in the NaOX solution. (a) $DO-H\cdots OD_2$; (b) $DO-H\cdots OD^-$; (c) $DOD\cdots O-H^-$. These are limiting cases; in reality, there may be intermediate cases as well with a more delocalized charge.

Up to now, most knowledge on the effect of OH^- ions in a liquid solution results from non-time-resolved experiments, such as infrared[108] and Raman[87] spectroscopy, dielectric relaxation,[12] and neutron diffraction.[11] Extensive data on the geometry and thermodynamic properties of the solvated OH^- ion are available from calculations; see for example Refs. 17, 99, 123, 127 and the references to experimental work therein. Direct information on the dynamics has only been provided by *ab initio* molecular dynamics simulations. These simulations showed that the structure of the hydrogen-bond network is strongly related to proton/deuteron transfer,[118,117] and they showed also to what extent the proton is delocalized in a $H_3O_2^-$ complex.[119]

In this paper, we study the microscopic structure and dynamics of water in a strongly alkaline solution. The method of choice is time-resolved mid-infrared spectroscopy, which will provide more knowledge on the dynamics and structure of the water molecules in this strongly alkaline environment than conventional non-time-resolved techniques.

6.2 EXPERIMENT

The experiments were pump–probe measurements where a femtosecond infrared laser pulse excited the $v = 0 \rightarrow 1$ transition of the OH stretch vibration in the NaOX solution. The transmittance of a subsequent probe pulse with an independently tunable frequency is a measure of the degree of excitation of the OH groups in the solution.

The general background on pump–probe experiments is discussed in §1.2, the details of the pulse generation in §2.2.4, and the pump–probe setup in §2.4.1. The sample consists of a 200 μm-thick layer of a 10 mol/l solution of NaOD in D_2O (a concentrated NaOD:D_2O solution was obtained from Sigma-Aldrich, which was appropiately diluted), in which a small amount of the deuterium was replaced by hydrogen, such that the transmittance of this sample in the range 2900–3600 cm^{-1} was approximately 4%, corresponding to a D:H ratio of about 100:1. The sample was at room temperature and at a fixed position in the laser beam focus. See §2.8 for an estimate of the thermal effects in such a sample.

In each measurement, we measured the absorbance change $\Delta\alpha(t)$ for a large number of delay values t, while we kept the pump and probe frequencies (ω_{pu} and ω_{pr}, respectively) fixed. This procedure was repeated for a number of pump and probe frequencies, which yielded a 3-dimensional data set $\Delta\alpha(\omega_{pu}, \omega_{pr}, t)$.

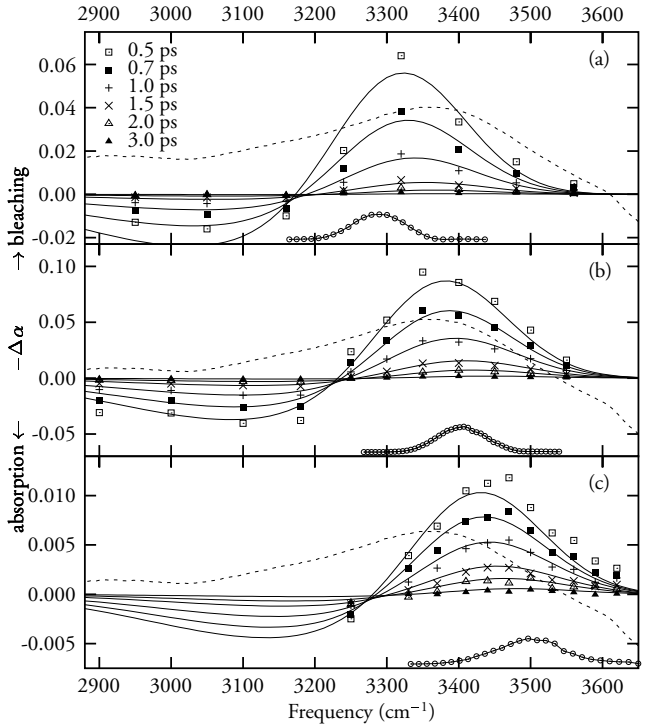

FIGURE 6.3. Transient spectra of the 10 M NaOX solution (data points) at several different pump–probe delays, for excitation at (a) 3290, (b) 3405, and (c) 3500 cm^{-1}. The data points at the bottom of each plot indicate the pump pulse spectra. The drawn curves result from Eq. (6.5) with the parameters from Table 6.1 and the dashed curves, also relative to the bottom of each plot, indicate the linear absorption spectrum (see also Fig. 6.1), that is obviously much broader than the bleaching bands.

6.3 RESULTS

6.3.1 TRANSIENT SPECTRA

By combining experimental data for different probe frequencies, we constructed transient spectra of the NaOX solution for excitation at pump frequencies $\omega_{pu} = 3290$, 3405, and 3500 cm^{-1}. Figure 6.3 shows these transient spectra for delays $t \geq 0.5$ ps. From these spectra it follows that the OH absorption band of the NaOX solution is strongly inhomogeneous: the bleaching signals are much narrower than the linear absorption spectrum and the frequency of the maximum bleaching signal depends strongly on the pump frequency, even at larger delay times ($\geq$ 2 ps). This means that the excitation leads to the formation of a spectral hole that persists on a picosecond timescale. This is in contrast to the situation in plain HDO:D_2O (see Refs. 33, 129 and Chapter 8), where such a strong dependence on the pump frequency exists only for delay times <1 ps.

The fact that the NaOX solution is inhomogeneous means that the absorption band in the linear spectrum in Fig. 6.1 corresponds to a population distribution function $f_i(\omega)$ that

represents the number of OH groups that absorb at a particular frequency ω. Excitation of a purely inhomogeneous system with a pump pulse spectrum $f_{\mathrm{pu}}(\omega)$ with a nonzero width results in a spectral hole with a line shape that is the product of $f_{\mathrm{i}}(\omega)$ and $f_{\mathrm{pu}}(\omega)$. If we assume that f_{i} and f_{pu} are Gaussians with central frequencies ω_{i} and ω_{pu} and widths (defined as the standard deviation of a Gaussian) Δ_{i} and Δ_{pu}, respectively, the spectral hole is a Gaussian with central frequency

$$\omega_{\mathrm{hole}} = \frac{\Delta_{\mathrm{pu}}^2}{\Delta_{\mathrm{pu}}^2 + \Delta_{\mathrm{i}}^2}\omega_{\mathrm{i}} + \frac{\Delta_{\mathrm{i}}^2}{\Delta_{\mathrm{pu}}^2 + \Delta_{\mathrm{i}}^2}\omega_{\mathrm{pu}}, \tag{6.2}$$

i.e. somewhere between ω_{i} and ω_{pu}, where we assume a sample with a weak absorption.[♩] The standard deviation of this Gaussian is $\Delta_{\mathrm{hole}} = \Delta_{\mathrm{i}}\Delta_{\mathrm{pu}}/(\Delta_{\mathrm{i}}^2 + \Delta_{\mathrm{pu}}^2)^{1/2}$, which is narrower than both Δ_{pu} and Δ. From the CW spectra in Fig. 6.1, we estimate $\omega_{\mathrm{i}} = 3370\ \mathrm{cm}^{-1}$ and $\Delta = 170\ \mathrm{cm}^{-1}$. With $\Delta_{\mathrm{pu}} = 34\ \mathrm{cm}^{-1}$ and $\omega_{\mathrm{pu}} = 3500\ \mathrm{cm}^{-1}$, we would expect a spectral hole centered at $\omega_{\mathrm{hl}} = 3495\ \mathrm{cm}^{-1}$, with $\Delta_{\mathrm{hl}} = 33\ \mathrm{cm}^{-1}$. This is nowhere near the experimental data in Fig. 6.3c, where the hole is centered at $3450\ \mathrm{cm}^{-1}$ and has a standard deviation of $\sim 98\ \mathrm{cm}^{-1}$ (corrected for the broadening effect of the probe pulse bandwidth). Therefore, there must be a broadening effect due to a rapid spectral modulation process. In other words, an individual molecule that was excited at a particular frequency subsequently affects the transient absorption at a slightly different frequency. The timescale of this spectral modulation process must be very short, because no significant broadening occurs after 0.5 ps.

6.3.2 The OH band as a distribution of Brownian oscillators

To describe an inhomogeneous distribution of OH groups that is subject to spectral modulation, we use the modified[129] Brownian-oscillator[88] model, of which details are given in §5.4, although it now applies to OH groups instead of OD groups. In the absence of vibrational relaxation, the bleaching signal at delay $t \geq 0$, with pump and probe frequencies ω_{pr} and bandwidths Δ_{pu} and Δ_{pr}, is given by Eq. (5.4), which we repeat here:

$$B(\omega_{\mathrm{B}}, \omega_{\mathrm{pu}}, \omega_{\mathrm{pr}}, t) = A\left[B_{01}(t) + B_{10}(t) - \sigma B_{12}(t)\right]. \tag{6.3}$$

Here, A is the amplitude of the signal that depends on how efficiently the pump pulse excites the ground-state molecules. The terms B_{ij} represent the contributions to the probe signal for the $v = i \rightarrow j$ transitions. Equation (6.3) describes the pump–probe signal for an ensemble of Brownian oscillators each of which has the same central frequency ω_{B} and in which there is no vibrational relaxation from the $v = 1$ to the $v = 0$ state. We saw in Chapter 4 that the vibrational lifetime T_1 depends on the OH stretch frequency ω_{B} as

$$T_1(\omega_{\mathrm{B}}) = \tau_{\mathrm{OH}}(1 - \omega_{\mathrm{B}}/\omega_{\mathrm{gas}})^{-1.8}, \tag{6.4}$$

where $\omega_{\mathrm{gas}} = 3707\ \mathrm{cm}^{-1}$ is the frequency of the OH stretch vibration in gas-phase HDO (Ref. 110) and τ_{OH} is a proportionality constant. To incorporate the inhomogeneous

[♩] For an optically thick sample (absorbance $\gg 1$), all pump energy would be absorbed, resulting in $\omega_{\mathrm{hole}} = \omega_{\mathrm{pu}}$ and $\Delta_{\mathrm{hole}} = \Delta_{\mathrm{pu}}$. In this case, the difference is negligible.

TABLE 6.1. Model parameters [Eqs. (5.1)–(5.11), (6.4)–(6.7)] for the NaOX solution. The parameter T_1' is discussed in §6.3.3. Section 6.3.4 describes how we obtained the parameter values.

Parameter		Value
Spectral correlation time[♭]	τ_c	0.05 ps
Band central frequency	ω_o	3332 cm^{-1}
Diffusive bandwidth[♯]	Δ_d	65 cm^{-1}
Inhomogeneous bandwidth[♯]	Δ_i	77 cm^{-1}
Anharmonic redshift	$\delta\omega_{anh}$	283 cm^{-1}
Stokes shift	$\delta\omega_{sto}$	20 cm^{-1}
R shift for $v = 2$ potential	a	2.6
$v = 1 \rightarrow 2$ relative cross-section	σ	1.5
Component I lifetime prefactor	τ_{OH}	6.7 fs
Component II decay time	T_1'	0.14 ps

[♭] Any value smaller than approximately 0.10 ps can describe the experimental data.
[♯] Bandwidths refer to standard deviations of Gaussian line shapes. To obtain the FWHM, multiply by 2.35.

character and the frequency-dependent relaxation time, we integrate Eq. (6.3) over the inhomogeneous line shape $f_i(\omega_B)$ and obtain the expression

$$S_I(\omega_{pu}, \omega_{pr}, t) = \int d\omega_B \, f_i(\omega_B) \, e^{-t/T_1(\omega_B)} \, B(\omega_B, \omega_{pu}, \omega_{pr}, t). \tag{6.5}$$

We assume here that, due to vibrational relaxation, the bleaching decays with a lifetime T_1. As discussed in Chapter 4, it is likely that the decay time of the bleaching is slightly longer than the 'true' vibrational lifetime, but in the remainder, we use the symbol T_1 for the decay time of the bleaching. Since we do not have any *a priori* information on the exact composition of the linear absorption spectrum of the NaOX solution in Fig. 6.1, we use a simple Gaussian

$$f_i(\omega_B) = \exp\left(-(\omega_B - \omega_o)^2/2\Delta_i^2\right) \tag{6.6}$$

for the inhomogeneous line shape in Eq. (6.5). We find that Eq. (6.5), convolved with the pump–probe pulse cross-correlate, can very well describe the experimental data in Fig. 6.3 with the parameter values in Table 6.1.

The effect of T_1 being frequency-dependent [Eq. (6.4)] is more clearly visible when we plot the bleaching signals as a function of delay. Figure 6.4 shows typical pump–probe delay scans at various $(\omega_{pu}, \omega_{pr})$ combinations. The experimental data show indeed a more rapid decay for lower probe frequencies than for higher frequencies, in both the bleaching band and the induced-absorption band. The frequency dependence of the vibrational lifetime causes the transient spectra to shift slightly towards higher frequencies with increasing delay, because the lower-frequency parts of both the bleaching bands and the induced-absorption bands decay slightly faster than their higher-frequency counterparts. This means also that the frequency with zero absorbance change shifts towards higher frequencies. This effect causes the singularities in the (logarithmically plotted) curves for $\omega_{pr} = 3250$ cm^{-1} in Fig. 6.4b and $\omega_{pr} = 3330$ cm^{-1} in Fig. 6.4c, which show a transition from bleaching to induced absorption. The delay value at which the bleaching and induced absorption at a particular frequency compensate each other is extremely sensitive to

the exact line shapes of the $v = 0 \rightarrow 1$ and $v = 1 \rightarrow 2$ contributions, which explains why the singularity in the experimental data and the model are at different time delays. The data for $\omega_{pr} = 3250$ cm^{-1} in Fig. 6.4b show an additional feature around $t = 0$ ps. The signal starts as a small induced absorption that changes into a bleaching at $t = 0$ ps. This is the effect of a negative and fast-decaying contribution that we will discuss in the next section.

6.3.3 Dynamics at small delays

The data in Fig. 6.4 deviate strongly from single-exponential decays. Nearly all measurements show a decay that is significantly faster at small delays. This fast initial decay is also visible for high pump and probe frequencies. Hence, the frequency dependence of T_1 as described by Eq. (6.4) cannot explain this initial decay. One might think that this fast initial decay results from to the spectral modulation of the Brownian oscillators. Spectral modulation implies that directly after excitation, a relatively narrow bleaching band appears in the transient spectrum, that subsequently broadens and decreases in amplitude. For equal pump and probe frequencies, the spectral modulation would thus cause an initially rapid decay of the absorbance change, since the decay is caused by both spectral diffusion and vibrational relaxation, while at larger delay times, the decay rate decreases. For pump and probe frequencies that differ, the initial decay would be slower, because then the molecules would diffuse into the spectral window of the probe: the decay caused by vibrational relaxation would (partially) be compensated. However, in many data sets where pump and probe frequencies differ, a fast initial decay is visible, comparable to the case where pump and probe are equal. Hence, spectral modulation cannot cause the the initial fast decay.

Interestingly, the initial fast decay has a rapid decay constant T_1' that is more or less independent of the pump and probe frequencies. In contrast, the amplitude of this fast component does depend on the pump–probe combination. We add the rapid decay as a phenomenological term to Eq. (6.5), which yields the absorbance change

$$\Delta\alpha(\omega_{pu}, \omega_{pr}, t) = -\left[c_I(\omega_{pu}) S_I(\omega_{pu}, \omega_{pr}, t) + c_{II}(\omega_{pu}, \omega_{pr}) e^{-t/T_1'}\right]. \qquad (6.7)$$

Here, $c_I(\omega_{pu})$ is an amplitude factor that depends on the exact pump intensity in the focus. The amplitude factor $c_{II}(\omega_{pu}, \omega_{pr})$ is different for each curve in Fig. 6.4. We convolve the above function (defined for $t \geq 0$) with the pump–probe pulse cross-correlate in order to account for the nonzero pulse duration. Thus, Eq. (6.7) describes pump–probe signals of a phenomenological fast decaying component (further denoted as component II) and an inhomogeneous distribution of Brownian oscillators (further denoted as component I) over frequencies ω_B with lifetimes T_1 that depend on the frequency ω_B. Component I includes the $v = 0 \rightarrow 1$, the Stokes-shifted $v = 1 \rightarrow 0$, and the anharmonically red-shifted $v = 1 \rightarrow 2$ transitions.

From fitting the experimental data (see §6.3.4), we find that component II has a lifetime $T_1' = 140 \pm 20$ fs. Figure 6.5 shows spectra of component II, which are qualitatively similar to the transient spectra of component I, with a bleaching at high frequencies and an induced absorption at lower frequencies.

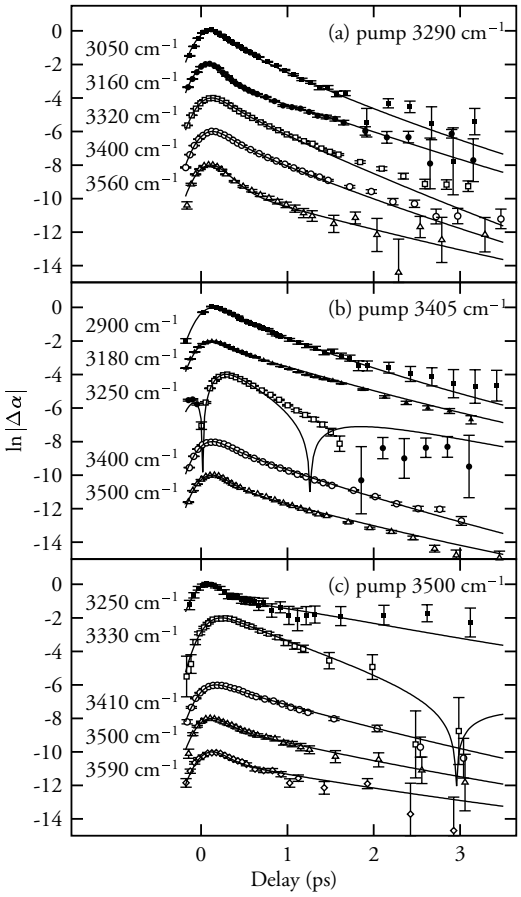

FIGURE 6.4. Pump–probe scans on the NaOX solution for a few different pump and probe pulse frequencies (data points). The data are plotted logarithmically as $\ln|\Delta\alpha|$. Data points with filled symbols correspond to induced absorption ($\Delta\alpha > 0$); open symbols correspond to bleaching ($\Delta\alpha < 0$). To aid comparison, the curves and data points are shifted vertically—the true amplitudes can be read from Fig. 6.3. The curves result from Eq. (6.7) with parameters from Table 6.1; the amplitudes of component II, which affects the signal for $t < 0.5$ ps, are shown in Fig. 6.5. For delays $t > 0.5$ ps, Eq. (6.7) and Eq. (6.5) do not differ significantly. The two curves with singularities are elucidated in the last paragraph of §6.3.2.

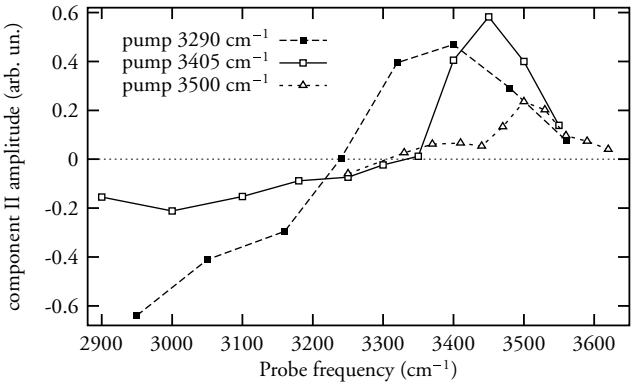

FIGURE 6.5. Transient spectra of component II, defined as the ratio c_{II}/c_I (c_I is the overall amplitude of the spectrum of component I).

6.3.4 FIT DETAILS

The parameters τ_c, $c_{II}(\omega_{pu}, \omega_{pr})$, and T_1' mainly affect the data for short delays. From the absence of broadening in time of the transient spectra in Fig. 6.3 for delays $t \geq 0.5$ ps, we conclude that the spectral correlation time τ_c [Eq. (5.3)] is shorter than the pulse duration (i.e. $\sim$250 fs).

For delays $t \geq 0.5$ ps, the shapes of the transient spectra are nearly entirely determined by component I, with parameters ω_o, Δ_d, Δ_i, $\delta\omega_{anh}$, a, τ_{OH}, τ_c, and $c_I(\omega_{pu})$. The Stokes shift $\delta\omega_{sto}$ follows from Δ_d [Eq. (5.2)]. In order to determine these parameters, we did a simultaneous least-squares fit on transient spectra at a large number of delays $t \geq 0.5$ ps, while we set $c_{II} = 0$ for all data sets.

Subsequently, we used the fit results in a simultaneous fit on the transients as a function of delay time (as in Fig. 6.4), where only c_I, c_{II}, and T_1' were allowed to vary. (c_I needs only minor adjustments to account for the spatial overlap between pump and probe pulses, that is not exactly the same for different probe frequencies.)

To determine how sensitive the fit results are for the exact value of τ_c, we repeated the entire fit procedure for $\tau_c = 0.05$, 0.1, 0.2, and 0.4 ps. This yielded very similar values for the parameters in Table 6.1, but caused c_{II} to have a physically highly improbable probe frequency dependence if $\tau_c > 0.10$ ps, with zero amplitudes at the central frequencies of the bleaching bands in Fig. 6.3. By virtue of Ockham's razor, we conclude therefore that $\tau_c \leq 0.10$ ps; we used the value $\tau_c = 0.05$ ps. The formal errors in the parameters in the fits were fairly small (typically a fraction 10^{-3} of the parameter value). However, the model assumes that the pulse spectra, pulse time envelopes, and inhomogeneous and diffusive bandwidths all have ideal Gaussian shapes. The fact that the true shapes are not Gaussian is most likely a more significant, but very difficult to calculate quantitatively, source of errors. Therefore, we do not show the formal errors, because these are not representative of the true uncertainties.

6.4 DISCUSSION

In plain HDO:D_2O, spectral diffusion covers the entire OH stretch absorption band of the linear spectrum, with a correlation time of ≈600 fs. Such a type of spectral diffusion is completely absent in component I of the NaOX solution, where the absorption spectrum is inhomogeneously broadened on at least a picosecond timescale. This means that the hydrogen-bond network, which is the main responsible for the spectrum of the OH stretch vibration, is effectively immobilized due to the presence of a high concentration of Na^+ and OX^- ions. Neutron diffraction experiments[11] recently showed that the O–O radial distribution function, which is related to the structure of the NaOX solution, is indeed very different from that of water. Apparently, the disturbed structure of the hydrogen-bond network allows only small fluctuations, that are very rapid, judging from the nearly instantaneous broadening of the spectral holes. The NaOX solution has a high density (62 M O atoms) with respect to plain water (56 M O atoms). However, this high density is not likely the direct cause of the slow hydrogen-bond dynamics; from the compressibility $\kappa = 45 \times 10^{-6}$ bar^{-1} (Ref. 72) of water, we can estimate that water reaches a 62 M O-atom density at a pressure of 2.6 kbar. From the neutron diffraction data,[11] the equivalent pressure was estimated to be even higher, 9 kbar. However, the reorientation time of water, that is closely related to the hydrogen-bond dynamics (changing the orientation of a water molecule requires stretching and/or breaking its hydrogen bond, see Chapter 7) changes by only ∼17% going from ambient pressure to 4 kbar, or by 20% at 9 kbar.[55] This small effect of the density is confirmed by the behavior of the viscosity. The viscosity of water, also related to the making and breaking of hydrogen bonds, increases by 20% and 80% for 4 and 9 kbar, respectively.[55] The viscosity of a 10 M NaOH solution is a factor 13.5 larger than the viscosity of pure water.[72] These considerations suggest that high charge density, rather than the high particle density, is responsible for the absence of sub-picosecond hydrogen-bond dynamics.

Additional support for the observed absence of hydrogen-bond dynamics is provided by data on the reorientation of OH groups in the NaOX mixture. We performed polarization-resolved measurements similar to the pump–probe delay scans in Fig. 6.4 on a 10 M NaOX solution, where we excited with a pump frequency of 3400 cm^{-1} and measured the absorbance change $\Delta\alpha(t)$ separately for parallel ($\parallel$) and perpendicular ($\perp$) probe polarizations. From these data, we calculated the rotational anisotropy,

$$A(t) = \frac{\Delta\alpha_{\parallel}(t) - \Delta\alpha_{\perp}(t)}{\Delta\alpha_{\parallel}(t) + 2\Delta\alpha_{\perp}(t)}. \tag{6.8}$$

The pump pulse preferentially excites OH groups that are approximately parallel to the polarization of the pump pulse, such that $A = 0.4$ at $t = 0$. The decay of A indicates to what extent the OH groups can change reorientation; free orientation motion would result in $A \to 0$. More details on this polarization-resolved technique will be discussed in Chapter 7. Figure 6.6 shows the decay of the anisotropy for probe frequencies centered at 3400 and 3280 cm^{-1}. Clearly, the decay of the anisotropy is limited to a small decrease at delays $t \lesssim 0.5$ ps, which indicates that each individual OH group can only change its orientation within a limited angular range. This observation is in contrast to similar experiments on HDO dissolved in D_2O, which we will discuss in detail in Chapter 7. In HDO:D_2O, the anisotropy decays with a time constant of 2.6 ps. The present limited

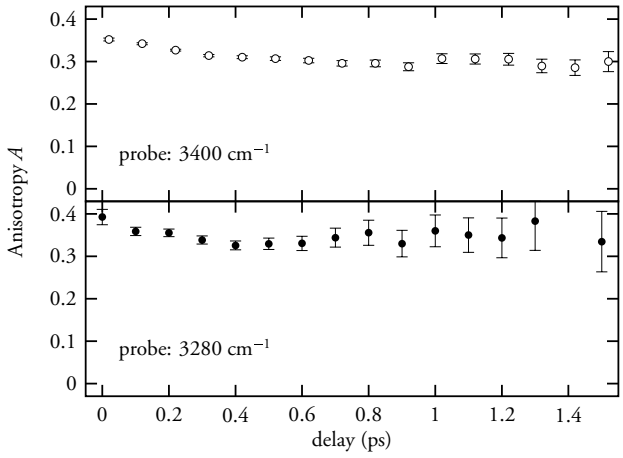

FIGURE 6.6. Rotational anisotropy of the 10 M NaOX mixture pumped at 3400 cm^{-1}. Only at small delays, a very small decay of the anisotropy is visible, after which the anisotropy stays nearly constant.

decay of the anisotropy is in agreement with the observed absence of hydrogen-bond dynamics, since large changes in the orientation of an OH group must involve stretching, making, and/or breaking of hydrogen bonds. We can therefore regard the structure of the hydrogen-bond network as a 'gel'-like state.

The small and rapid fluctuations in the immobilized hydrogen-bond network in the NaOX solution are represented by the Brownian-oscillator model [Eq. (6.5)]. These fluctuations cause a spectral modulation with a correlation time τ_c and an (unknown) amplitude Δ_m around the central frequency ω_B of each OH group. This spectral modulation results in an almost instantaneous broadening of the spectral holes; the line shape of this broadening has a width defined by Δ_d. We remark that our modelling assumes a relatively slow spectral modulation, i.e. the quantity $\epsilon \equiv \tau_c\Delta_m$ is $\gg 1$, in which case $\Delta_m \approx \Delta_d$. However, the value range $\tau_c \leq 100$ fs implies that $\epsilon \leq 1.2$. Therefore, the interpretation of Δ_d requires additional attention. It is impossible to know from the present experimental data whether (1) $\epsilon \ll 1$ or (2) $\epsilon \approx 1$. Case (1) would mean that the line shape of the broadening is the Lorentzian $(1 - \omega^2/\Delta_h^2)^{-1}$ with a half-width $\Delta_h = \epsilon\Delta_m$, which is narrower than Δ_m due to motional narrowing. In this limit, we should compare the value $\Delta_d = 65$ cm^{-1} to the homogeneous broadening Δ_h due to pure dephasing (commonly written as $\Delta_h = 1/T_2^*$), with the remark that the present model assumes Gaussian line shapes instead of Lorentzian line shapes. Homogeneous broadening is always instantaneous and not dependent on the pump–probe delay. In this case, Δ_m is unknown because it depends on the unknown value of τ_c. Case (2) is the intermediate modulation regime, where the line broadening is almost instantaneous and the line shape of the broadening is between a Gaussian and a Lorentzian, with width defined by Δ_d, with $\Delta_d < \min(\epsilon, 1)\Delta_m$.

Recently, infrared photon-echo experiments[115] showed that the absorption band of the OH stretch vibration of HDO in D_2O contains a homogeneously broadened component

with a half-width $\Delta_h = 60$ cm^{-1}, where it was estimated that $\tau_c \sim 30$ fs. Likely, the rapid fluctuations that are responsible for the instantaneous broadening in the NaOX solution are of the same nature as those causing the homogeneous broadening in HDO:D_2O. This is in good agreement with our finding that $\tau_c < 100$ fs and $\Delta_d = 65$ cm^{-1}. This homogeneous broadening can also explain why Eq. (6.5) systematically yields amplitudes that are too small at the high-frequency side of the transient spectra in Fig. 6.3: the tails of a Gaussian lineshape (as in the model) are smaller than those resulting from $\epsilon \sim 1$. However, it is not likely that the line shape is purely homogeneously broadened ($\epsilon \ll 1$), since the resulting Voigt lineshape [i.e., a convolution of a Lorentzian with a half-width of 65 cm^{-1} (due to spectral modulation) and Gaussian with a half-width of 77 cm^{-1} (due to the inhomogeneous distribution)] would have a significant absorbance around 3700 cm^{-1} in the linear spectrum.

Apparently, component II consists of a class of OH groups that differ from those in component I in that they have a very fast vibrational relaxation (~0.14 ps). Their transient spectra (Fig. 6.5) show both bleachings and induced absorptions at frequencies similar to those of component I (curves in Fig. 6.3), which suggests that these OH groups have O–H···O hydrogen bond lengths similar to those of component I. Therefore the mechanism of vibrational relaxation of component II must be different from that of component I or that of water (see Chapter 4). Since, apart from the absence of spectral diffusion, component I behaves similarly to HDO in D_2O, it is likely that component I corresponds to HDO molecules that are hydrogen bonded to D_2O molecules (Fig. 6.2a). Component II is likely related to OH groups of HDO molecules that are hydrogen-bonded to OD^- ions, as in Fig. 6.2b. According to *ab initio* molecular dynamics simulations on the solvation of OD^- (Ref. 117, 118), there are two solvation structures of the OD^- ion: (a) $D_9O_5^-$, which is relatively stable, and (b) $D_7O_4^-$, in which rapid deuteron hopping can occur. Structures (a) and (b) transform into each other typically every 2–3 ps. The deuteron transfers in structure (b) occur typically with intervals of 40–100 fs and require only very small changes of the positions of the individual oxygen atoms. At each deuteron transfer, a D_2O molecule is transformed into an OD^- ion (and vice versa), which effectively changes the position of the complex in the global hydrogen bond network, since with each hop, one D_2O molecule leaves the complex and another enters. Such a deuteron transfer has a strong impact on any excited OH vibrations in participating HDO molecules, as the hydrogen bonds inside the complex are shorter ($R = 2.6$ Å) than between the surrounding water molecules (2.8 Å). This change in hydrogen-bond length corresponds to large jumps in the OH frequency, and is apparently accompanied by a rapid vibrational relaxation. Since this mechanism means that excitation at 3030 cm^{-1} should result in a bleaching at much higher frequencies, we have done an experiment in which we excited the NaOX solution at 3030 cm^{-1} and where we probed at 3330 cm^{-1} (Fig. 6.4). Indeed, the excitation results in a bleaching that decays rapidly, with a rate comparable to that of component II. This provides support for the hypothesis that component II consists of HDO molecules that are affected by deuteron hopping.

It is interesting to note that the linear absorption spectrum in Fig. 6.1 is much wider (~400 cm^{-1} FWHM) than one would expect from the convolution of the diffusive and inhomogeneous bandwidths of component I (i.e. 235 cm^{-1} FWHM). This is in agreement with the picture that component II has a very broad spectral distribution that apparently contributes significantly to the linear spectrum. Further, the fact that the components I

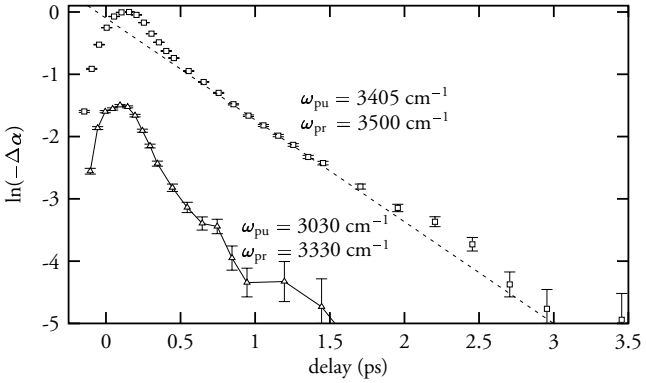

FIGURE 6.7. Pump–probe transients with different pulse frequencies. Pumping at 3030 cm^{-1} results in a bleaching at 3330 cm^{-1} that has a decay rate comparable to component II. The line is a guide to the eye to indicate a purely exponential decay ($\tau = 0.61$ ps).

and II are so distinctly visible in the experimental data suggests that very little exchange between component I and II occurs, even though there is one OX^- ion available for every 5.6 water molecules, of which 3 or 4 are needed to form the $HD_6O_4^-$ or $HD_8O_5^-$ complexes. It seems therefore that the deuteron exchange in component II is confined to certain regions in the hydrogen bond network, and that deuteron exchange is not possible to other regions, that constitute component I.

Of course on a longer timescale exchange does occur, which may be responsible for the fact that, for equal frequencies, the vibrational lifetime T_1 of component I is somewhat faster than in HDO:D_2O, i.e. 0.6 ps versus 0.74 ps, both at 3400 cm^{-1}. A small amount of exchange would not be directly visible in the transient spectra in Fig. 6.3, since any excited OH group that switches from component I to component II would disappear almost instantaneously due to the fast relaxation of component II. Vice versa, the bleaching signal of component II does not live long enough to influence component I significantly.

6.5 CONCLUSIONS

We have shown that the linear absorption spectrum of the OH stretch vibration of HDO molecules in a 10 M NaOD in D_2O solution consists of two components. Component I consists of HDO molecules that are hydrogen bonded as $DO{-}H\cdots OD_2$ (Fig. 6.2a). These differ from HDO molecules dissolved in D_2O, because the OH groups in component I do not show slow spectral diffusion ($\tau_c \approx 600$ fs for HDO:D_2O), they have a lower central frequency (3332 cm^{-1} instead of 3400 cm^{-1}), and they have a vibrational relaxation rate that is slightly faster. Component II consists of HDO molecules such as in Fig. 6.2b, that participate in deuteron hopping between OD^-/OH^- ions and HDO/D_2O molecules, which is accompanied by large jumps in the frequency. These molecules show a very rapid vibrational relaxation. The difference in vibrational relaxation rates between HDO in D_2O and HDO in the NaOX solution suggests that there is a small amount of exchange between components I and II. This small amount of exchange and the absence

of spectral diffusion in component I on the experimental picosecond time scale show that the structure of the hydrogen bond network is very static in the NaOX solution.